

A Computation Effective Range-based 3D Mapping Aided GNSS with NLOS Correction Method

Hoi-Fung Ng¹, Guohao Zhang¹ and Li-Ta Hsu¹

1 Interdisciplinary Division of Aeronautical and Aviation Engineering, The Hong Kong Polytechnic University

(E-mail: lt.hsu@polyu.edu.hk)

Global navigation satellite system (GNSS) positioning in dense urban areas is still a challenge due to the signal reflection by buildings, namely the multipath and non-line-of-sight (NLOS) receptions. These effects degrade the performance of low-cost GNSS receiver (e.g., smartphone). An effective 3D mapping aided GNSS positioning method is proposed to correct the NLOS error. Instead of applying ray-tracing simulation, the signal reflection points are detected based on a skyplot with the surrounding building boundary. Therefore, the measurements of the direct and reflected signals can be simulated and further used to determine the user's position based on the measurement likelihood between real measurements. Verified with real experiments, the proposed algorithm is able greatly lower the computation load while maintaining the positioning accuracy as 10m error in dense urban, comparing to conventional ray-tracing-based NLOS corrected positioning method.

KEYWORDS

3DMA GNSS, NLOS, Urban Canyon, 3D building model

1. INTRODUCTION. Accurate positioning is essential for smartphone users. The positioning solution of the smartphone is mainly determined by a low-cost built-in global navigation satellite system (GNSS) receiver. With the differential Global Navigation Satellite System (DGNSS) correction, the smartphone can achieve positioning solution within 1 to 2 meters of error in open areas. However, the urban area is still a challenging environment with the majority of smartphone users, usually suffering dozens of meter positioning error (Dabove and Petovello, 2014; Pesyna et al., 2014). In the urban area, the GNSS signal can be blocked or reflected by the building surface. Hence, both the direct and reflected signals or only the reflected signals are being received, namely the multipath and non-light-of-sight (NLOS) reception respectively

(Groves, 2013). The extra travelling distance of the reflected signal can further introduce a large error during positioning, possibly exceeds 50 meters, as the major error source of GNSS urban positioning especially in deep urban canyons (Hsu, 2018).

Since the smartphone can intelligently determine the environment class that is located in, the specific algorithm for GNSS-challenged environments should be developed (Gao and Groves, 2018). To improve the urban GNSS positioning accuracy, different researches focused on the exclusion of NLOS affected measurement. The consistency-check method (Groves and Jiang, 2013) is used to detect and isolate the unhealthy pseudorange measurements, achieving a satisfactory positioning result. However, the performance may degrade in the dense urban scenario with severe NLOS reception. Multiple NLOS receptions as the outliers may lead to fault consistency issue, degrades the correctness of fault detection and exclusion (Hsu et al., 2017). A method using the sky-pointing fisheye camera to detect the NLOS signal by image recognition (Moreau et al., 2017; Suzuki and Kubo, 2014) also introduced. Another approach is using the 3D light detection and ranging (LiDAR), the NLOS signals can be detected (Wen et al., 2018b) and corrected based on scanned surrounding building distance and NLOS propagation model (Wen et al., 2018b; Wen et al., 2018a). However, it requires extra equipment and power consumption which are not practical for hand-held devices.

To prevent adding extra equipment and make use of all the received measurements, the 3DMA (3D mapping-aided) GNSS positioning algorithms as NLOS-excluded positioning (Obst et al., 2012), shadow matching (Wang et al., 2013; Groves, 2011) and ray-tracing (Hsu et al., 2016a; Miura et al., 2015), were proposed to improve the positioning in dense urban areas. The shadow matching uses the building boundaries from the 3D city model and the position of the satellite from the ephemeris to estimate the satellite visibility of a specific location. The shadow matching uses the building boundaries (Wang et al., 2012), the highest elevation angle of the surrounded building on each azimuth angle, from the 3D city model and the position of the satellite from the ephemeris to predict the satellite visibility of a specific location. Therefore, the user position can be determined by the candidate location with a satellite visibility best matching the measurements. It can effectively improve the positioning accuracy on the across-street direction. However, it is less effective for along-street direction, due to the similarity of building geometry (Adjrad and Groves, 2018a). As shadow matching only provides a partial solution, a likelihood-based 3DMA GNSS ranging method is demonstrated to focus on the use of measurements on the along-street direction (Groves and Adjrad, 2017). With their complementary characteristics, the integration of the likelihood-based 3DMA GNSS and GNSS shadow matching is proposed in (Adjrad and Groves, 2018a). Recently, the implementation of the integrated method is tested on an Android device (Adjrad and Groves, 2018b). To improve the positioning solution in both along-street and across-street directions, the UCL integrated solution is introduced. The entire scope of works with performance analysis are presented in (Groves and Adjrad, 2019) and (Adjrad et al., 2019). One idea is not only to

detect the NLOS measurement but also correct it. Ray-tracing based 3DMA GNSS positioning algorithms were developed to detect and correct the reflected signal on NLOS and multipath propagation. This method traces the possible transmission route of both direct and reflected GNSS signals based on 3D building models. Hence, the pseudorange error from reflection can be simulated and further corrected to improve positioning accuracy. This approach can estimate the NLOS reception error precisely for correction, providing a positioning accuracy about 10m or lower (Miura et al., 2015). With NLOS correction, affected measurements become useful for positioning, which gives a better dilution of precision (DOP) and sufficient measurement amount even in dense urban. The integration of 3DMA GNSS with inertial sensors for pedestrian and vehicle applications are introduced in (Suzuki and Kubo, 2013), (Hsu et al., 2016b) and (Gu et al., 2016), respectively. However, the ray-tracing algorithm requires a high computation load since it performs the comparison between simulated pseudorange and measurements (Ziedan, 2017). This criteria lead to a high-performance computing platform to apply this algorithm, which is not feasible real-time positioning by a smartphone. As a result, to perform an accurate positioning method without intensive computation load is desired. For the ray-tracing approach, numbers of candidates are firstly distributed around. Then, the transmission path of each signal is simulated on every surface at each candidate, which are computationally expensive. Furthermore, the positioning performance also depends on level of detail (LOD) of 3D building model (Biljecki et al., 2014), and consideration of multiple reflections.

This paper develops a new 3DMA GNSS positioning method based on the enhanced skymask, which includes the building boundaries as well as the building height information to provide the NLOS corrections, and details will be described in section 3.2. The main contributions of the proposed 3DMA GNSS method are: 1) reducing the computation load while maintaining similar performance as the ray-tracing algorithm, within 5 meters extra positioning error comparing to ray-tracing; and 2) using the same format of building boundary used in GNSS shadow matching to correct NLOS measurements. The proposed method is a position hypothesis-based estimation method. To estimate the NLOS pseudorange delay in each hypothesized-position, we propose to use the characteristic of perfect reflection where the incidence angle is identical with the reflection angle. The elevation angle of reflecting point is equal to that of satellite. Where the reflecting surface is parallel to the direction of travel, the azimuth of the reflecting point position with respect to the direction of travel is equal and opposite to the azimuth of the satellite with respect to the direction of travel, in here, we named it as the azimuth angle of the reflecting plane (AARP), as Figure 5. Therefore, innovatively, based on the enhanced skymask and the satellites position, we can determinate the reflecting plane direction AARP and predict the incoming signal direction. With the building height from enhanced skymask, the exact coordinate of the reflecting point can be further obtained. With the characteristic of NLOS signal transmission and reflected by the reflector, this assumption

avoids searching the appropriate reflection point on each building surface, which significantly decreases the computation requirements comparing to ray-tracing based 3DMA GNSS. This simplification still maintains the accuracy of reflected signal simulation regarding the conventional approach. To conclude, the proposed simplified ray-tracing NLOS correction algorithm is applicable for smartphone achieving real-time accurate positioning solution in dense urban with the presence of many unhealthy measurements.

The preliminary result is reported in (Ng et al., 2019). However, in the previous work, the parallel direction in azimuth angle (from north) of the reflecting planes, as the AARP in section 3.2, of the surrounded building surfaces are labelled manually. We further propose a new algorithm to identify different surfaces in the skymask. As a result, the proposed method can be tested in more complicated building distribution environments comparing to that in (Ng et al., 2019).

2. OVERVIEW OF THE PROPOSED 3DMA GNSS ALGORITHM. Figure 1 shows the flowchart of the proposed algorithm. The algorithm can be divided into two main parts, offline and online processes, offline process is precomputed on the server while online process is processed by the receiver after receiving the GNSS measurements.

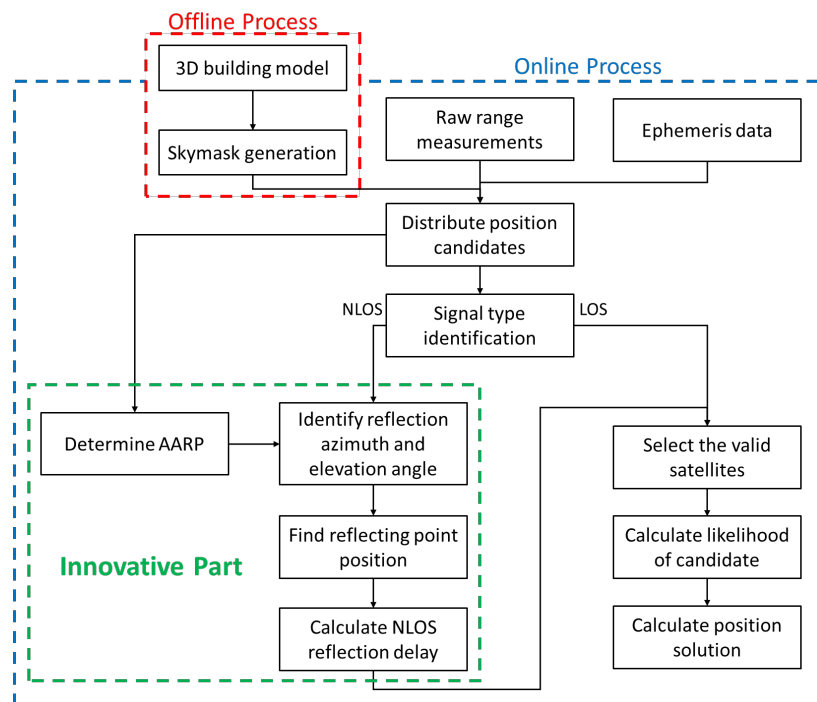


Figure 1 - Flowchart of the proposed range-based 3DMA GNSS algorithm

The offline process is to generate the building boundaries on skyplot, and named ‘enhanced skymask’ in this paper. The skymasks are stored in a specific format inside the receiver with resolution 1-degree for azimuth angle; the elevation angle is 0.1-degree. For practical implementation, the skymasks can be downloaded from the server from time-to-time to reduce

the storage requirements for storing a wide area of skymasks. For the online process, position candidates are distributed evenly around an initial position. For each candidate, the azimuth angle of the reflecting planes (AARP) will be found on each corresponding azimuth angle by candidate's skymask and feature points. The AARP value on each azimuth means the parallel direction of the surrounded building surface, also known as a possible surface for reflection occur, on the corresponding azimuth. This value used to predict the azimuth angle and will be explained in section 3.2. Meanwhile, for each candidate position, satellites are placed on the skymask to identify whether it will be blocked by the building. For the NLOS measurements, the possible reflecting point can be found based on the azimuth and elevation angles relationship between the receiver, satellite, and the law of reflection, the detailed processes on identify the reflecting point are stated on section 3.2. Therefore, the reflection delay can be estimated and correct the NLOS measurement. After that, if the type of measurement is agreed by both skymask classification and signal strength classification, it is identified as a valid measurement for the candidate, as state in Table 1. The simulated pseudorange is calculated for each valid satellite on each candidate. Then, compare the similarity between measured and simulated pseudorange. A scoring scheme based on the average of pseudorange difference on each candidate is applied to score candidate. A higher score is given to the candidate position with a higher similarity between measured and simulated pseudorange. Finally, the solution is estimated by weighted averaging the scored position candidates.

3. ALGORITHM DESCRIPTION. The algorithm description can be divided into three main parts, the skymask generation, reflecting point detection, and positioning with simulated range.

3.1. Skymask Generation. In the offline stage, the building boundaries are projected on the skyplot, also named 'skymask' in this paper. If the satellite elevation is lower than the building boundary elevation (under the same azimuth angle), the signal is assumed to be the NLOS signal blocked by buildings.

The skymask of each location is generated with the 3D city model offline, as show in Algorithm 1. Thus, the skymask can be initially stored in the device. Based on the 3D building model or in storage perspective, a specific area is selected and divided into grid points to construct the skymask table, the grid point separation is 2m to generate the skymask. Here, an assumption is made. The candidate always stays to the ground (mean-sea-level). Therefore, the height of the skymask position is given by the mean-sea-level datum by the Hong Kong Lands Department (1995). The Figure 2 is an example on the generated skymask and storage format. The azimuth is in 1-degree resolution; the elevation is in 0.1-degree resolution; and the building height is in 1-m resolution. The azimuth angle starts from the north direction, rotating in clockwise direction; the elevation angle starts from the horizon as 0° .

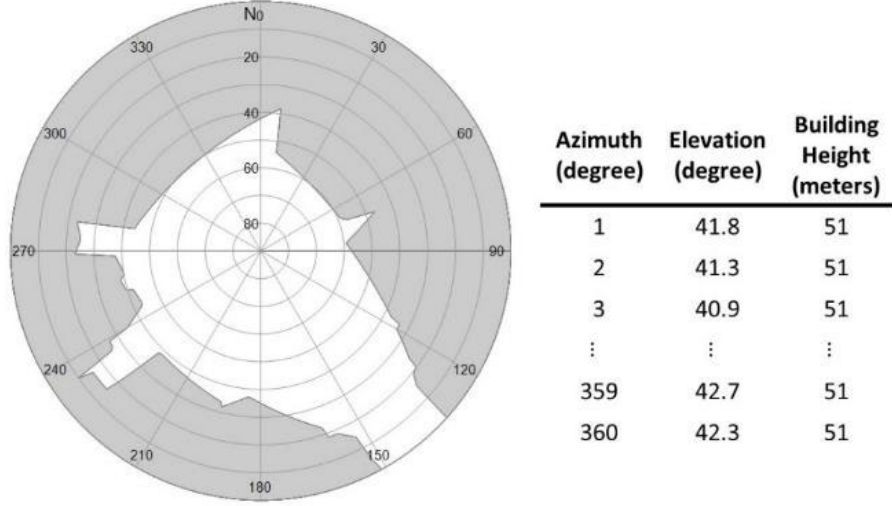


Figure 2 - Example of skymask (left) and skymask array (right)

Algorithm 1: Skymask generation on a specific location

Input: Location, P

3D building model, vertexes of buildings in ECEF

stepping distance, ϵ , in meter, represent the accuracy when searching the building-edge

Output: Enhanced skymask list \mathbf{S} (including 360 of rows on corresponding azimuth angle, with 2 columns)

- 1st column, $\mathbf{S}(az, 1)$: elevation angle on corresponding azimuth angle az

- 2nd column, $\mathbf{S}(az, 2)$: building height on corresponding azimuth angle az

- 1 Sort the buildings by the distance between the location, from the nearest to farthest
 - 2 **for** each building i
 - 3 **for** each building vertex j
 - 4 calculate j and $j+1$ vertex azimuth (with respect to the north) and elevation angle from location P
 - 6 initial temp location along the building edge T' be vertex j
 - 7 **if any**(elevation of the corresponding azimuth in skymask list < elevation angle of j and $j+1$ vertex)
 - 8 **while** distance between vertex j & $j+1$ < distance between T' & vertex j
 - 9 calculate the azimuth az' and elevation el' angle at T'
 - 10 **if** $\mathbf{S}(az') < el'$
 - 11 update $\mathbf{S}(az', 1)$ value to el' and $\mathbf{S}(az', 2)$ to building height h
 - 12 **end if**
 - 13 update location T' by step up ϵ along direction vertex j to $j+1$
 - 14 **end while**
 - 15 **end if**
 - 16 **end for** each building vertex j
 - 17 **end for** each building i
-

Each location will be firstly classified whether it is inside the building. For the ‘outside building’ location, a list of total 360-degree will be used to store the maximum elevation angle of building edge for corresponding azimuth angle. As well as the building height on the corresponding azimuth, as shown in Figure 2, for later use to find the valid reflecting point; for the ‘inside building’ location, a flag will be given to represent this is a building.

This offline generation perspective is especially important for a low-cost device with limited computational power. As these devices are nearly impossible to generate the skymask every time neither in time consumption nor power management aspect. This step is similar to the process that the study proposed in (Wang et al., 2012), but the enhanced skymask includes the building height information that associated with each azimuth angle for NLOS correction usage.

3.2. Detection of Reflecting Points on Skymask. In the real-time positioning, theoretically, an initial position is firstly given by single point positioning (SPP) at each epoch to distribute positioning candidates around. To provide a more sophisticated initial solution, the NMEA position provided by the receiver will be used in this paper. By a grid of searching area with 40m radius and 2m separation between adjacent candidates will be constructed. Since the skymask information is pre-computed based on grids, distributing the candidate in the same grids makes it feasible to directly load the corresponding skymask information and avoids applying interpolation. If the candidate is distributed inside the building, it will not calculate its likelihood. Then, the satellites are projected on the skyplot of each candidate based on their position estimated using ephemeris data, as well as loading the corresponding skymask. As a result, the satellites can be classified into LOS and NLOS from the candidate skymask. Figure 3 shows the flow to determine the reflecting point from the skymask for NLOS satellite.

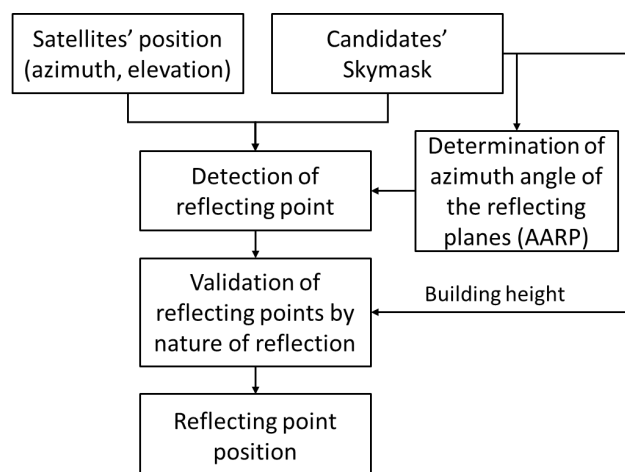


Figure 3 - Flowchart on reflecting point detection

With the skymask information of the candidate, we should determine the AARP value on each surrounding building surface, as Algorithm 2 shown. The geometry meaning is the parallel

direction of the building surface that the reflection occurs. The AARP value, φ , is the building surface's parallel direction in azimuth angle with respect to north in the clockwise direction, as Figure 5 shown. Noted that the AARP value determination can be processed on offline stage by server or online stage by the receiver. The advantage of processing by the server when generating skymask is that it can get the AARP value directly by the 3D building model. While the advantage for online calculation is that it can reduce the required storage on the receiver, as the AARP value on each grid need to be store with the skymask if calculate offline.

Algorithm 2: AARP-based possible reflected signal incoming direction prediction

Input: Enhanced skymask \mathbf{S} of the candidate position

Output: AARP $\varphi = \{\varphi_{az} | az = 1^\circ, 2^\circ, \dots, 360^\circ\}$, possible reflected signal incoming direction $\psi = \{\psi_{az} | az = 1^\circ, 2^\circ, \dots, 360^\circ\}$ with regarding to different azimuth direction az

- 1 **for** $az = 1^\circ \rightarrow 360^\circ$
- 2 Obtain the corresponding elevation el_{az} from \mathbf{S}
- 3 **if** adjacent elevation difference $\Delta el_{az, az+1} > 2^\circ$
- 4 Sudden change points $\leftarrow az$
- 5 **end if**
- 6 **end for**
- 7 Local minima/Local maxima \leftarrow the az that slope equal to 0 and not labelled Sudden change points
- 8 Feature points $\mathbf{az}^* \leftarrow$ Sudden change points, Local minima, Local maxima
- 9 **for** each feature point $az_k^* \in \mathbf{az}^*$
- 10 Obtain the corresponding elevation $el_{az_k^*}$ and building height $h_{az_k^*}$ from \mathbf{S}
- 11 Compute the candidate-to-feature-point distance $d_{az_k^*} = h_{az_k^*} / \sin(el_{az_k^*})$
- 12 Convert feature point from polar coordinate $(el_{az_k^*}, az_k^*, d_{az_k^*})$ to local coordinate (x_k, y_k, z_k) :
 - 13 North $x_k = \cos(az_k^*) \cos(el_{az_k^*}) d_{az_k^*}$
 - 14 East $y_k = \sin(az_k^*) \cos(el_{az_k^*}) d_{az_k^*}$
 - 15 Down $z_k = -h_{az_k^*}$
- 16 **end for**
- 17 **for** $az = 1^\circ \rightarrow 360^\circ$
- 18 obtain the adjacent feature points fulfill $az \in [az_k^*, az_{k+1}^*]$
- 19 Compute the corresponding AARP $\varphi_{az} = \text{atan2}(y_{k+1} - y_k, x_{k+1} - x_k)$
- 20 Compute the corresponding possible reflected signal incoming direction $\psi_{az} = 2\varphi_{az} - az$
- 21 **end for**

Unlike the 3D building model used in the ray-tracing 3DMA GNSS (Hsu et al., 2016a), surrounded buildings are mixed together in the skymask and not separable. Thus, it is important to identify the individual building surface since each surface may have different AARP. The building boundary on the skymask can be illustrated as a curve with respecting to the elevation

and azimuth as Figure 4. As shown in Figure 5, the corresponding AARP needs to be identified to estimate the valid reflecting point for a different building.

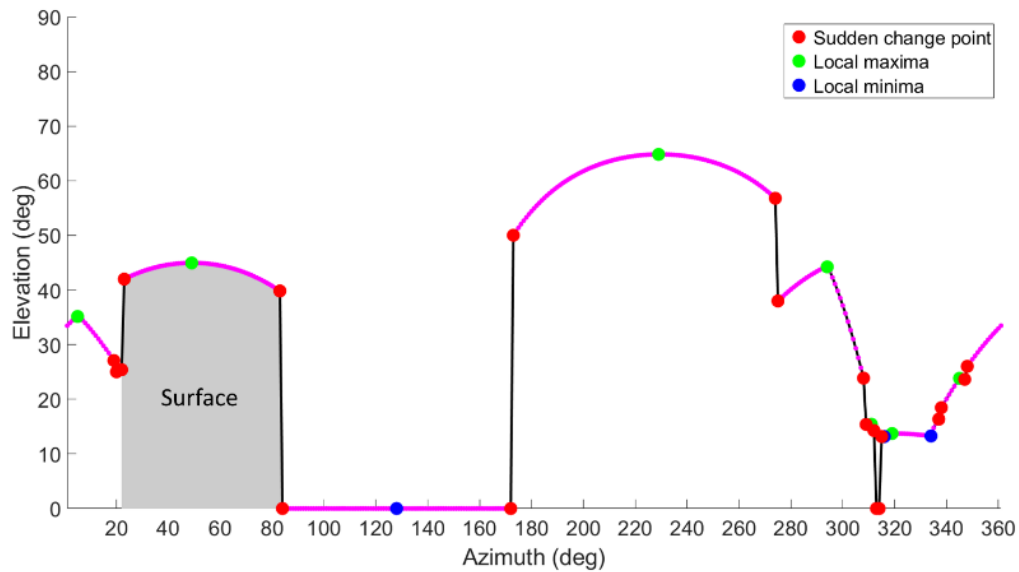


Figure 4 - Skymask (the right of Figure 5) plot in elevation-azimuth format and determined feature points. Red, green, blue points are feature points; purple lines represent valid surface; black lines are invalid surface; grey shadowed area is the blue surface in Figure 5

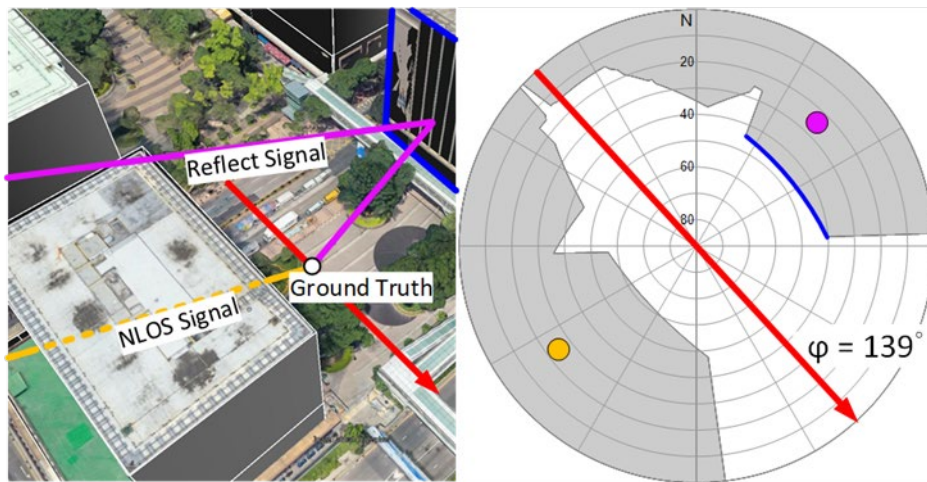


Figure 5 - Actual position (left) and their polar position projected on skymask (right), red arrow is the AARP for the blue surface that reflection occurs and φ is the axis direction angle; orange line is the direct path blocked by building; purple line is the reflecting path. Orange and purple point on skymask represent the signal incoming azimuth and elevation angle of the direct and reflected path respectively

Two features from the skymask curve are extracted to determine the corresponding AARP of the potential reflect surface. The first feature is the sudden changing point, corresponding to the building boundary points with over 2-degree elevation angle difference between two adjacent points. The curve between two sudden changing points indicates the transition to different buildings, which is invalid for signal reflection. The skymask curve with small change (less than 2-degree) represents a valid surface for signal reflection. The second feature is the

local minima or maxima within the valid curve. The feature points could be representing the different visible surface from the candidate.

Follow by identifying the valid surface and its orientation from the skymask. As mentioned above, the feature points represent the building corner. Therefore, the azimuth angles between two consecutive feature points will consider as one surface. While two exception case, if two adjacent azimuth angles (e.g. az & $az + 1$) are sudden change point, which means this change to another building and should be no surface exists, will not consider as a surface. Another situation is the elevation is 0-degree, as it is assumed to be no valid reflector on the ground.

After obtaining the feature points including sudden change points, local minima and local maxima, the AARP on each azimuth angle are computed by two adjacent feature points. Then the possible reflected signal incoming direction ψ_{az} regarding to the building surface on different azimuth direction az can be computed with step 21 in Algorithm 2. Therefore, for a specific satellite i , the corresponding signal reflecting point azimuth can be obtained by matching the known satellite azimuth az^i with the predicted possible reflected signal incoming direction, as follows

$$az_{RefI}^i = \arg \min_{az \in \{1^\circ, 2^\circ, \dots, 360^\circ\}} (\psi_{az} - az^i) \quad (1)$$

Noted that if no existing ψ_{az} fulfills $|\psi_{az} - az^i| < 1^\circ$ for a satellite at a candidate, no valid reflecting signal can be found for this satellite on this candidate position.

The AARP determination algorithm aims to provide a more accurate possible reflection surface determination based on skymask, the results can be illustrated using Figure 6 and 7. In Figure 6 environment, the orientation of the red surface is different from other surface. The actual AARP of surrounded surface are expressed with the purple arrows on Figure 6. The purple arrows on Figure 7 show the determined AARP by our proposed algorithm. From the results, the algorithm can identify correct AARP of surrounded surface, as well as some small visible surface form location's skymask.

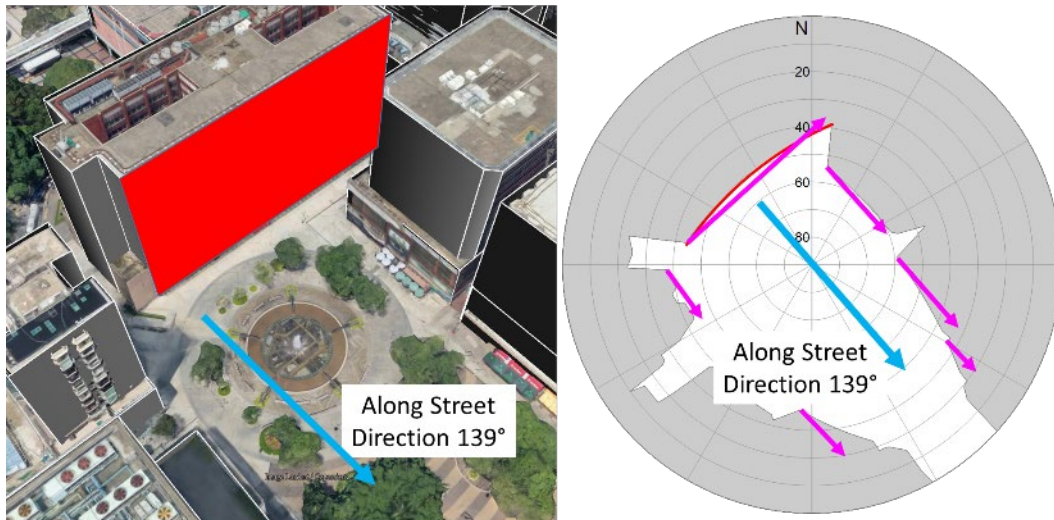


Figure 6 - Complex environment (left) with multiple axis directions and corresponding skymask (right). Blue arrow is the along street direction; purple arrows are the surround visible surface AARP; the red curve on the right represents the red surface on the left

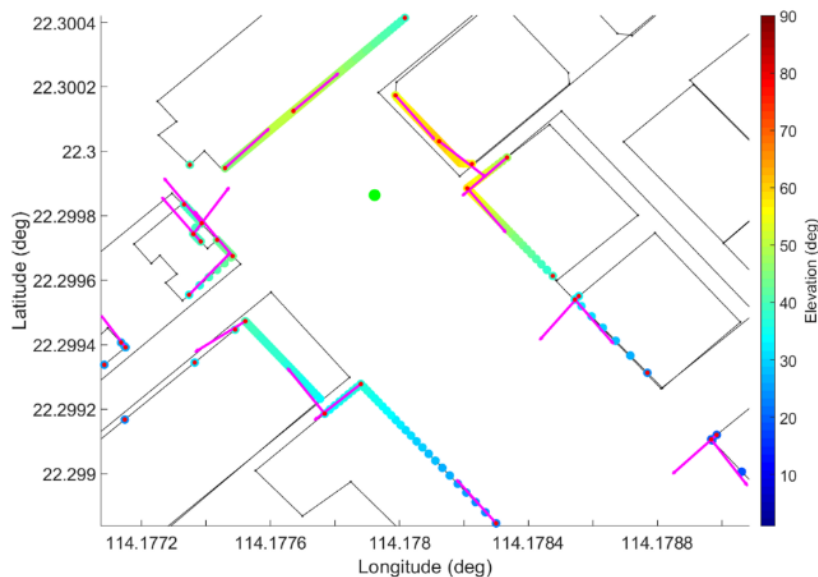


Figure 7 – Demonstration of the result by the proposed AARP algorithm. Green point is the ground truth location in Figure 6; black solid line is the building contour; colour points are the location used on the skymask, the colour represents the elevation angle; purple arrows represent the AARP vector determined by propose algorithm

As indicated in (Hsu, 2018), NLOS delay can be modelled with elevation angle and lateral distance from the receiver to the reflector. Therefore, after determining the AARP and predicting the incoming signal direction with candidate's skymask, we can detect the reflecting points and output actual position.

Before detecting the reflecting point from the AARP we found in the above step, we need to know the angular relationship between the receiver, satellite position and AARP. As shown in

Figure 8(a), the satellite elevation at the receiver is the same as at the reflecting point provided that the reflecting surface is vertical, since the satellite is far away from the reflecting point and receiver. With the law of reflection, the incident angle is equal to the reflection angle which is the elevation angle of reflecting point, as θ_{elev} . On the other hand, on the view from the above of the receiver as Figure 8(b), an AARP is defined parallel to the building surface that reflect the NLOS signal. Since the satellite is far away from the receiver and the reflecting point, the incident reflected signal (from satellite to reflected plane) is parallel to the direct signal, making the angle between reflected plane and incident reflected signal (or $90^\circ - \text{incident angle}$) equals the azimuth angle between the AARP and the direct signal, as γ_{azi} . Due to pure reflection behavior, the incident angle is equal to the reflection angle, which is also equal to the azimuth angle between the reflecting point and the AARP (which is parallel to the reflecting surface). Therefore, the location of the reflecting point can be estimated by the satellite elevation and azimuth angles with respect to the receiver in the skymask. As Figure 5 shows, based on the preceding relationship, the valid reflecting point (purple point) of the GNSS signal on the building surface can be determined symmetrically to the satellite position (orange point) on the skymask with respect to the AARP.

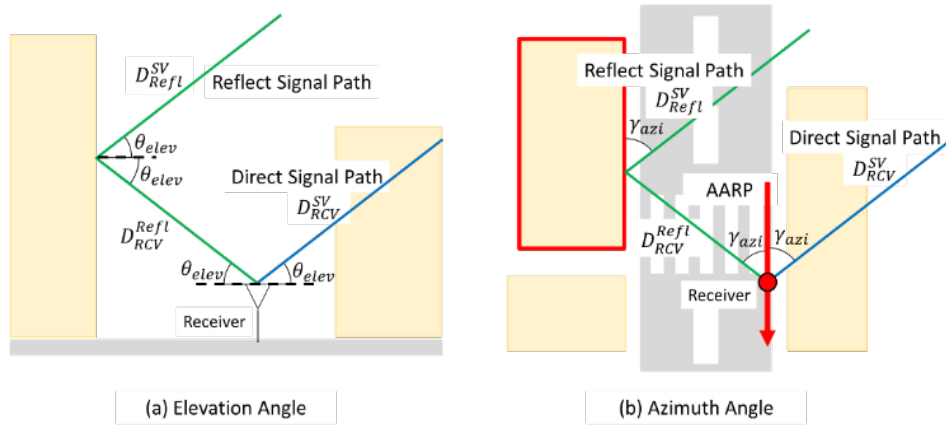


Figure 8 - (a): side view to demonstrate the angular relationship between the direct and reflected signal on elevation; (b): top view to demonstrate the azimuth angle relationship. Green and blue line represent reflect and direct path respectively; red arrow is the AARP of reflection occur surface (red framed building)

Finally, the horizontal distance from candidate to building height on the corresponding reflecting point's azimuth can be resolved by building height and elevation angle to the building edge. By further combining with the azimuth and elevation angle of the reflecting point, the actual position of the reflecting point can be obtained by converting from local coordinate to ECEF using the standard coordinate transformation matrix.

As well as the reflection delay of i -th satellite on n -th candidate, $\epsilon_n^{refl(i)}$, from the total geometric distance of the reflect path (1. Satellite to reflecting point, D_{Refl}^{SV} ; and 2. Reflecting point to the receiver, D_{RCV}^{Ref}) then subtract the geometric distance of direct LOS path, D_{RCV}^{SV} .

$$\varepsilon_n^{refl(i)} = D_{RefI}^{SV} + D_{RCV}^{RefI} - D_{RCV}^{SV} \quad (2)$$

3.3. *Simulated Range Calculation.* To evaluate the likelihood of the position candidates, the difference between pseudorange measurement $\tilde{\rho}$ and simulated range $\hat{\rho}$ on each position candidate are required. The simulated range $\hat{\rho}_n^i$ between the i -th satellite and the n -th position candidate can be calculated by the sum of the geometric distance R_n^i , correction for satellite clock and orbit offset, $c\delta t_i^{sv}$, ionosphere errors (using the Klobuchar model (Klobuchar, 1987)), I^i , and troposphere errors, T^i and reflection delay distance, $\varepsilon_n^{refl(i)}$ found in section 3.2 if applicable, as following,

$$\hat{\rho}_n^i = R_n^i + c\delta t_i^{sv} + I^i + T^i + \varepsilon_n^{refl(i)} \quad (3)$$

To eliminate the receiver clock offset, a reference satellite will be selected. All measurements and simulated ranges, are differenced once to obtain the single difference (SD) of the ranges on each candidate. The reference satellite $r(i)$ is selected by the LOS satellite with the highest elevation angle for each constellation on each candidate. Noted that inter-constellation timing bias could be obtained from the broadcast navigation message. In the case, we can consider all the measurements are from the same constellation.

$$D_n^i = \left| \left(\tilde{\rho}_n^i - \tilde{\rho}_n^{r(i)} \right) - \left(\hat{\rho}_n^i - \hat{\rho}_n^{r(i)} \right) \right| \quad (4)$$

The similarity of the candidate α^n is calculated by averaging SD range differences. Table 1 shows the rule of signal type classification, the measurements can be classified into LOS and NLOS by the machine learning suggested by (Sun et al., 2018) and the prediction by the enhanced skymask. This classification applies to each candidate and measurement individually. If and only if the satellite agrees between the proposed method and signal strength classification, it will include in likelihood calculation for this candidate, the N_{sim} denotes the number of valid range differences. Noted that if the reference satellite is the only satellite that agrees on signal type, this candidate will not be scored and labelled as invalid.

$$\alpha^n = N_{sim}^{-1} \times \sum_i^{N_{sim}} D_n^i \quad (5)$$

Table 1 - Signal classification rule based on machine learning classification and enhanced skymask prediction

Enhanced skymask prediction			
LOS	Multipath	NLOS,	NLOS,

				no reflection found	reflection found
Machine learning classification	LOS	Valid	Valid	Invalid	Invalid
	NLOS	Invalid	Invalid	Invalid	Valid

The average of range difference will then rescaling between 0 to 1 to become the score of the candidates. A smaller value of the average of the range differences, the higher score is. In other words, the simulated range is more matching with the measurement.

$$score^n = \frac{\max(\alpha) - \alpha^n}{\max(\alpha) - \min(\alpha)} \quad (6)$$

The final step is to determine the position solution of the skymask 3DMA algorithm. All the candidates' score is then calculating the weighted average position. As a result, the positioning solution can be obtained. And the positioning solution will apply the height information from the pre-computed skymask grid point information.

$$x(t) = \frac{\sum_n(score^n(t)P^n(t))}{\sum_n score^n(t)} \quad (7)$$

4. EXPERIMENTS RESULTS AND ANALYSIS. To evaluate the performance of the proposed algorithm, experimental data were collected in urban canyons in Hong Kong and post-processed. The experiments involved the 'tidy' environment with few AARP directions and the complex environment with multiple axes.

4.1 Experiment Setup. A commercial-grade GNSS receiver (u-blox EVK-M8T with u-blox ANN-MS patch antenna) is used to record raw measurements. The output rate of the receiver is set with 1 Hz. The constellations on single-frequency GPS and BeiDou are enabled. Also, the static experiment 2 include the measurements recorded by Xiaomi Mi 8. The experiment results are then post-processed by quad-core i7 7th generation CPU, and comparing the positioning results on these algorithms:

- 1) WLS: weighted-least-square (WLS) (Realini and Reguzzoni, 2013)
- 2) RT: ray-tracing based 3DMA GNSS (Hsu et al., 2016a)
- 3) SKY: Skymask based 3DMA GNSS, the proposed method in this paper

Both the ray-tracing algorithm and the proposed Skymask based 3DMA GNSS consider the single reflection only, and provide correction only for the reflection-found NLOS signals. The

difference between the proposed and ray-tracing algorithm is the proposed one uses the skymask to obtain the NLOS correction. Therefore, we can evaluate the accuracy of the proposed method comparing with ray-tracing.



Figure 9 - Experiment locations: (a) Tsim Sha Tsui (b) Tsuen Wan, Hong Kong.

One dynamic and one static experiments were taken in the Tsim Sha Tsui (TST), Hong Kong; and one static experiment was taken in Tsuen Wan (TW), as shown in Figure 9. The referencing ground truth of each experiment is manually labelled based on the Google Earth. The ground truth of dynamic experiment, uniform velocity is assumed when doing the experiment, so ground truth is given by interpolating between starting point and destination with the total experiment time. The dynamic experiments took 69 seconds with about 70 meters walking distance. While the static experiments conducted 2 minutes (120 epochs). The experiments environment can be described as Table 2 show. In terms of the proposed axis determination method, the environment of experiment 1 is relatively simple compared to that of experiment 3.

Table 2 - Experiment environment

Experiment	Street width (m)	building height to street width ratio	Skymask elevation angle at ground truth		AARP determination error at ground truth	
			Mean (deg)	S.D. (deg)	Mean (deg)	S.D. (deg)
1	66	0.71	40.9	15.5	4.9	15.2
2	66	0.71	49.5	30.1	5.3	22.6
3	13	2.29	52.9	20.7	6.9	18.5

Noted that the building height to street width ratio is calculated by *building height/street width*, which means that the value is higher, the street is narrower with taller building surrounded and the experiment environment is more challenging for positioning. The ‘AARP determination error at ground truth’ is evaluated by comparing the AARP derived from the proposed method in section 3.2 with the AARP obtained from the 3D building model in Google Earth, and further demonstrated by mean value and standard deviation of the difference among all azimuth angles.

4.2 NLOS Reflection Detection and Correction Accuracy. Here will use the static experiments 2 and 3 ground truth to execute the skymask and ray-tracing based 3DMA GNSS methods to see whether the proposed method provides a consistent reflection delay distance comparing to ray-tracing prediction results. Table 3 and Table 4 includes the total signal which labelled as NLOS where reflection found or not by both methods. Total 1371 and 1345 signals found in TST and TW static experiments, respectively.

Table 3 - LOS/NLOS signal labelling in TST static experiment 2

		Proposed Skymask based 3DMA GNSS		
		LOS	NLOS (No Reflection found)	NLOS (Reflection found)
Ray-Tracing	LOS	960	42	0
	NLOS (No Reflection found)	0	118	42
	NLOS (Reflection found)	0	89	120

Table 4 – LOS/NLOS signal labelling in TW static experiment 3

		Proposed Skymask based 3DMA GNSS		
		LOS	NLOS (No Reflection found)	NLOS (Reflection found)
Ray-Tracing	LOS	696	203	70
	NLOS (No Reflection found)	0	193	125
	NLOS (Reflection found)	0	8	50

From the above result, the signal classification correct rate was about 87% and 70% in TST and TW, respectively. However, there were some signal miss-labeled, the ray-tracing classified as LOS while the skymask 3DMA classified as NLOS with no reflection found, as these signals direct path were stuck too near the building. This shows a potential problem of skymask on handling with the building edge model uncertainty, where some of the signals may miss detected if it is near the building edge. As a result, there is a difference in classifying the signal

type. While another main issue, the ray-tracing labeled as NLOS with no reflection found and the skymask method labelled as NLOS with reflection found. The main reason is the ray-tracing assumes the perfect single reflection, which two parts of the reflected signal path (1. Satellite to reflecting point; and 2. Reflecting point to the receiver) are not blocked by any buildings. However, the skymask method did not verify the path from satellite to reflecting point is free of blockage, so result in miss-identify reflection found.

Furthermore, the evaluation on the range level correction is needed, we will use the ground truth of the experiment, and perform the 3DMA GNSS to extract the NLOS range correction and compare with the double difference. Where the NLOS correction should be similar to the double difference residual if it is accurate enough. Using the satellite BeiDou B11 in TST (experiment 2) and BeiDou B7 in TW (experiment 3) to further analysis the NLOS correction accuracy in range level, we will give the comparison on NLOS correction between:

- 1) NLOS delay by double differencing technique (Xu et al.)
- 2) Proposed skymask 3DMA
- 3) Ray-tracing

The reflection correction of the proposed method can achieve a similar result to the ray-tracing one, the mean and S.D. of correction difference between skymask 3DMA and ray-tracing for BeiDou B11 in TST are 2.02m and 0.01m respectively, and the average difference between skymask 3DMA and double difference are 3.75m with S.D. 2.35m. While the mean difference between skymask 3DMA and ray-tracing of BeiDou B7 in TW is 1.84m with 0.00m deviate; the average difference between skymask 3DMA and the double difference is 1.58m with S.D. 1.46m. While other corrections provide by skymask 3DMA also comparable to the ray-tracing one, average within about 10m difference.

Table 5 summarize mean and S.D. of the NLOS delay from the proposed skymask 3DMA method and ray-tracing method for two satellites among all the satellites as examples. The performance is further compared with the NLOS delay estimated by double difference technique using the reference station data and user true location. It can be observed that proposed skymask 3DMA can provide a similar accuracy in range-level correction compare to the ray-tracing and actual measurement.

Table 5 - Summarize on NLOS reflection delay identified by three methods

Satellite	NLOS correction methods	Mean (m)	S.D. (m)
BeiDou B11	D.D. estimated delay	44.77	4.24
	Proposed skymask 3DMA	46.23	0.09
	Ray-tracing	44.20	0.08
BeiDou B7	D.D. estimated delay	8.15	2.17
	Proposed skymask 3DMA	8.13	0.01

	Ray-tracing	6.29	0.00
--	-------------	------	------

4.3 Positioning Results. The dynamic experiment was taken in TST, shown in Figure 10 and Table 6. The u-blox receiver collects the raw measurements during walking along the designed path to simulate a pedestrian scenario.

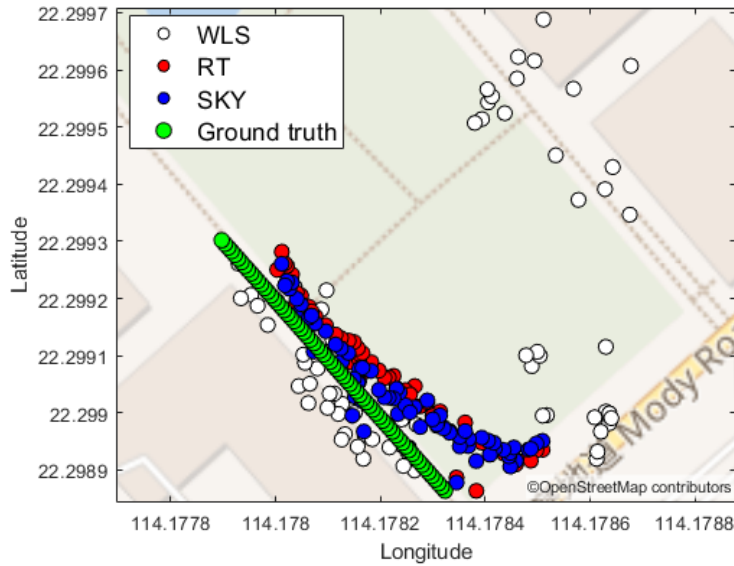


Figure 10 - Dynamic experiment results in TST

Table 6 - Dynamic experiment results in TST (unit: meter)

	2D-Error (m)			Along-Street Error (m)			Across-Street Error (m)		
	Mean	S.D.	RMS	Mean	S.D.	RMS	Mean	S.D.	RMS
WLS	27.65	24.02	36.51	9.32	5.72	10.91	24.39	25.06	34.84
RT	15.42	2.17	15.57	12.57	2.78	12.86	7.98	3.65	8.76
SKY	16.26	2.33	16.43	13.76	3.32	14.15	6.66	5.07	8.34

The along-street direction of the dynamic experiment is 139° and this angle is used to analyze the positioning error in the along-street and across-street directions. It can be observed that the overall performance of our proposed skymask 3DMA GNSS is over 10m better than the WLS solution in mean error. The proposed skymask 3DMA GNSS has an about 1m extra error on

the 2D and along-street direction, while the across-street direction can achieve similar accuracy compared to the ray-tracing algorithm.

The second experimental data was taken by the u-blox and Xiaomi Mi 8. This static data duration is 240 seconds. The positioning results and statistic shown in Figure 11 and Table 7, respectively.

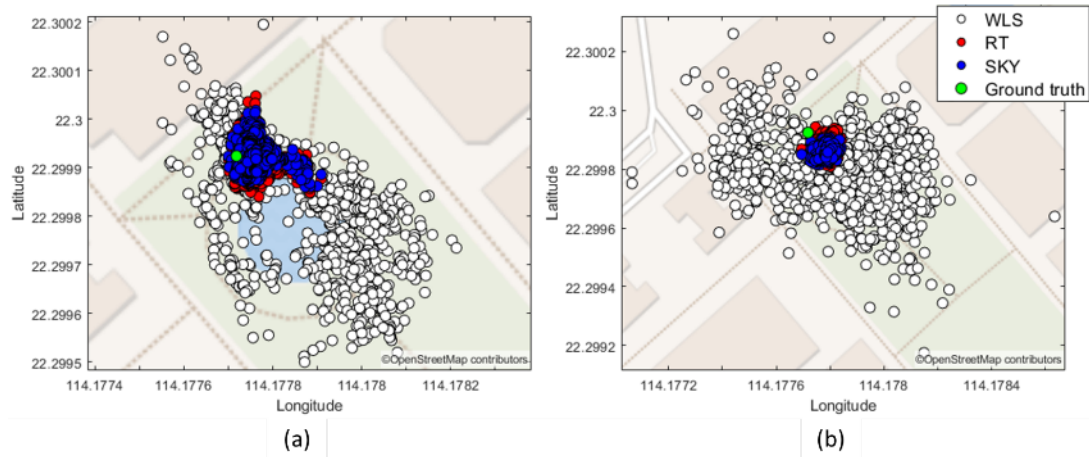


Figure 11 - Static experiment results in TST. (a) data recorded by u-blox; (b) data recorded by Xiaomi Mi 8

Table 7 - Static experiment results in TST by u-blox and Mi 8

		2D-Error (m)			Along-Street Error (m)			Across-Street Error (m)		
		Mean	S.D.	RMS	Mean	S.D.	RMS	Mean	S.D.	RMS
u-blox	WLS	20.71	16.13	26.24	18.70	16.31	24.81	6.41	5.65	8.55
	RT	6.09	2.91	6.75	4.52	2.87	5.36	3.30	2.43	4.10
	SKY	5.73	2.51	6.26	3.95	2.54	4.70	3.45	2.28	4.13
Mi 8	WLS	30.67	11.97	32.92	24.62	14.38	28.51	13.07	10.03	16.47
	RT	7.65	2.02	7.91	7.07	1.92	7.33	2.38	1.81	2.99
	SKY	10.18	1.52	10.30	9.96	1.56	10.09	1.65	1.25	2.07

From the positioning results, the Skymask 3DMA GNSS algorithm can achieve similar positioning results comparing to the ray-tracing based 3DMA GNSS algorithm for the u-blox

receiver. Especially the across street direction the RMS error of Skymask 3DMA is better than that of the ray-tracing algorithm. While the Mi 8 positioning results get worse than the ray-tracing in 2D and along street error, but the across street obtain slightly better than ray-tracing. In Figure 12, this static experiment took place in TW with u-blox only. The experiment environment is the densest urban area with only 10m width street, and the building height to street ratio is 2.29. Besides, the experiment located on the intersection of street that is in perpendicular. Therefore, the environment may be possible with multiple axes. And the positioning error statistic is shown in Table 8.

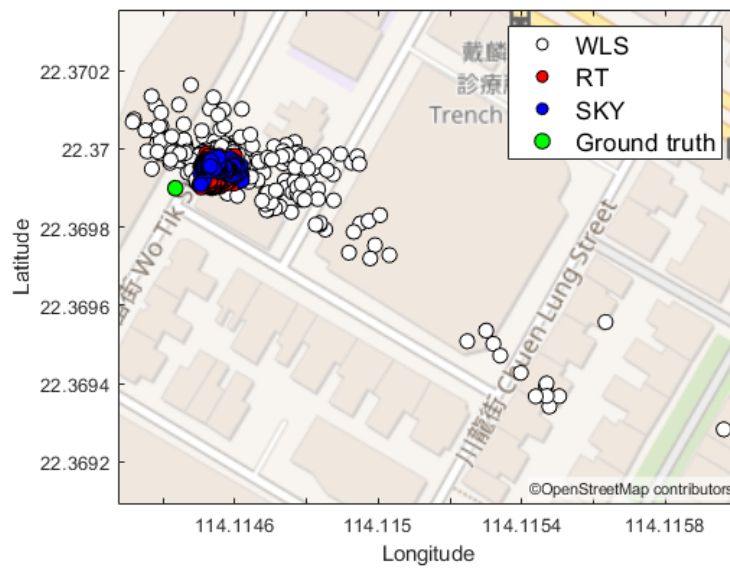


Figure 12 - Static experiment results in TW

Table 8 - Static experiment results in TW (unit: meter)

	2D-Error (m)			Along-Street Error (m)			Across-Street Error (m)		
	Mean	S.D.	RMS	Mean	S.D.	RMS	Mean	S.D.	RMS
WLS	30.28	26.02	39.88	15.40	6.85	16.84	23.08	27.89	36.15
RT	7.57	2.67	8.03	6.10	2.51	6.59	4.15	1.94	4.58
SKY	12.72	3.09	13.09	10.82	1.82	10.97	6.34	3.29	7.14

In this experiment, the skymask method can also achieve a similar accuracy compared to that of the ray-tracing. The 2D error is about 12m for the skymask method, 10m and 6m error on

along and across direction respectively. While the ray-tracing 2D error is 8m, 6m and 4m error on along and across direction respectively.

4.4 Computation Load. The post-processing time for the experiments is done by an Intel 7th Generation Intel® Core™ i7 Processors, with Matlab programming platform. The skymask 3DMA is about 10 times faster than ray-tracing in single epoch positioning. Table 9 summarize the average processing time for post-processing for different positioning algorithms

and the time reduction. The ‘Reduction on percentage’ is calculated by $\frac{t_{RT} - t_{SKY}}{t_{RT}} \times 100\%$

where t_{RT} and t_{SKY} are the average processing duration for on epoch for ray-tracing and skymask 3DMA respectively. The ‘Difference of 2D RMS Error’ is calculated by $RMS_{SKY} - RMS_{RT}$, where RMS_{RT} and RMS_{SKY} are RMS error of ray-tracing and skymask 3DMA respectively, the negative value here, extra positioning error of skymask 3DMA obtained.

Table 9 - Average processing time for experimental data

Experiment	Number of epochs	Average processing duration for one epoch (seconds)		Reduction percentage (%)	Difference of 2D RMS Error (m)
		Skymask 3DMA	Ray-tracing		
1 (u-blox)	69	8.83	62.30	85.83	+0.86
2 (u-blox)	1086	6.04	82.52	94.11	-0.49
2 (Mi 8)	1086	8.89	77.56	88.54	+2.39
3 (u-blox)	214	2.72	34.56	92.13	+5.06

5. CONCLUSIONS AND FUTURE WORK. This paper proposes a new method using the enhanced skymask, including the building boundary and height information, to estimate the possible reflecting point for NLOS reception. Based on the valid reflecting point and the signal classification scheme, the pseudorange measurements with NLOS delay are simulated for different candidate positions. The similarity between the measurements and simulated pseudorange with NLOS correction is then regarded as the score of the position candidate. By weighted averaging the candidate positions with scores, the receiver location can be better estimated in the urban scenario. Comparing with the ray-tracing, the proposed algorithm can provide similar NLOS correction with much lower computation load without extra equipment, which has the potential being applicable for portable devices.

However, the proposed skymask based 3DMA GNSS positioning still has limitations. The overlap of building surfaces in the enhanced skymask may cause misdetection of the reflecting surface, which needs to be intelligently separated without adding much computation load. Also, the proposed method does not consider the double-reflected GNSS NLOS that frequently observed in dense urban canyons (Hsu and Kamijo, 2015), which is possibly contained in the no-reflection-found NLOS part in Table 3 and 4. The exclusion (Hsu et al., 2015) or correction (Gu and Kamijo, 2017) of the double-reflected NLOS measurement can further improve the performance of 3DMA GNSS. Besides, the verification of the path from the satellite to the reflecting point being free of blockage needs to be further investigated. Comparing to the likelihood-based 3MDA GNSS ranging method (Groves and Adjrad, 2017), the proposed method considers additional information (e.g. the geometry relationship between reflection and building surface), resulting in a higher computation load. Even though the proposed method has significantly reduced the computation load comparing to ray-tracing algorithm, a further reduction of the processing time is still necessary to guarantee its feasibility for practical real-time applications. A straight-forward solution currently is to employ servers instead of the personal device to handle the computation load. In the near future, with the benefits from the computation load reduction, the algorithm could resolve the problem by considering multiple reflections of the signal path to enhance the NLOS correction accuracy.

REFERENCES

- (1995) Explanatory Notes on Geodetic Datums in Hong Kong. In: Survey and Mapping Office LD (ed). Hong Kong Special Administrative Region.
- Adjrad M and Groves PD. (2018a) Intelligent Urban Positioning: Integration of Shadow Matching with 3D-Mapping-Aided GNSS Ranging. *Journal of Navigation* 71 (1): 1-20.
- Adjrad M and Groves PD. (2018b) Real-Time 3D Mapping Aided GNSS on and Android Devices. *Proceedings of the 31st International Technical Meeting of the Satellite Division of The Institute of Navigation (ION GNSS+ 2018)*. Miami, Florida: Institute of Navigation (ION), 345-356.
- Adjrad M, Groves PD, Quick JC, et al. (2019) Performance assessment of 3D-mapping-aided GNSS part 2: Environment and mapping. *Navigation* 66 (2): 363-383.
- Biljecki F, Ledoux H, Stoter J, et al. (2014) Formalisation of the level of detail in 3D city modelling. *Computers, Environment and Urban Systems* 48: 1-15.
- Dabove P and Petovello MG. (2014) What are the actual performances of GNSS positioning using smartphone technology? *Inside GNSS* 9: 34-37.
- Gao H and Groves PD. (2018) Environmental Context Detection for Adaptive Navigation using GNSS Measurements from a Smartphone. *Navigation* 65 (1): 99-116.

- Groves P. (2013) Multipath vs. NLOS signals. *Inside GNSS* 8: 40-42.
- Groves PD. (2011) Shadow Matching: A New GNSS Positioning Technique for Urban Canyons. *Journal of Navigation* 64 (3): 417-430.
- Groves PD and Adjrard M. (2017) Likelihood-based GNSS positioning using LOS/NLOS predictions from 3D mapping and pseudoranges. *GPS Solutions* 21 (4): 1805-1816.
- Groves PD and Adjrard M. (2019) Performance assessment of 3D-mapping-aided GNSS part 1: Algorithms, user equipment, and review. *Navigation* 66 (2): 341-362.
- Groves PD and Jiang Z. (2013) Height Aiding, C/N0 Weighting and Consistency Checking for GNSS NLOS and Multipath Mitigation in Urban Areas. *Journal of Navigation* 66 (5): 653-669.
- Gu Y, Hsu L and Kamijo S. (2016) GNSS/Onboard Inertial Sensor Integration With the Aid of 3-D Building Map for Lane-Level Vehicle Self-Localization in Urban Canyon. *IEEE Transactions on Vehicular Technology* 65 (6): 4274-4287.
- Gu Y and Kamijo S. (2017) GNSS positioning in deep urban city with 3D map and double reflection. *2017 European Navigation Conference (ENC)*: 84-90.
- Hsu L-T. (2018) Analysis and modeling GPS NLOS effect in highly urbanized area. *GPS Solutions* 22 (1): 7.
- Hsu L-T, Gu Y and Kamijo S. (2015) NLOS Correction/Exclusion for GNSS Measurement Using RAIM and City Building Models. *Sensors (Basel, Switzerland)* 15 (7): 17329-17349.
- Hsu L-T, Hu Y and Kamijo S. (2016a) 3D building model-based pedestrian positioning method using GPS/GLONASS/QZSS and its reliability calculation. *GPS Solutions* 20 (3): 413-428.
- Hsu L-T and Kamijo S. (2015) NLOS Exclusion using Consistency Check and City Building Model in Deep Urban Canyons. *Proceedings of the 28th International Technical Meeting of the Satellite Division of The Institute of Navigation (ION GNSS+ 2015)*: 2390-2396.
- Hsu L, Gu Y, Huang Y, et al. (2016b) Urban Pedestrian Navigation Using Smartphone-Based Dead Reckoning and 3-D Map-Aided GNSS. *IEEE Sensors Journal* 16 (5): 1281-1293.
- Hsu L, Tokura H, Kubo N, et al. (2017) Multiple Faulty GNSS Measurement Exclusion Based on Consistency Check in Urban Canyons. *IEEE Sensors Journal* 17 (6): 1909-1917.
- Klobuchar JA. (1987) Ionospheric Time-Delay Algorithm for Single-Frequency GPS Users. *IEEE Transactions on Aerospace and Electronic Systems* AES-23 (3): 325-331.
- Miura S, Hsu L-T and Chen F. (2015) GPS Error Correction With Pseudorange Evaluation Using Three-Dimensional Maps. *IEEE Transactions on Intelligent Transportation Systems* 16 (6): 3104-3115.
- Moreau J, Ambellouis S and Ruichek Y. (2017) Fisheye-Based Method for GPS Localization Improvement in Unknown Semi-Obstructed Areas. *Sensors* 17 (1): 119.

- Ng H-F, Zhang G and Hsu L-T. (2019) Range-based 3D Mapping Aided GNSS with NLOS Correction based on Skyplot with Building Boundaries. *ION Pacific PNT 2019*. Manuscript submitted.
- Obst M, Bauer S and Wanielik G. (2012) Urban multipath detection and mitigation with dynamic 3D maps for reliable land vehicle localization. *Proceedings of the 2012 IEEE/ION Position, Location and Navigation Symposium*. 685-691.
- Pesyna KM, Heath RW and Humphreys TE. (2014) Centimeter Positioning with a Smartphone-Quality GNSS Antenna. *Proceedings of the 27th International Technical Meeting of The Satellite Division of the Institute of Navigation (ION GNSS+ 2014)*. Tampa, Florida, 1568-1577.
- Realini E and Reguzzoni M. (2013) Gogps: open source software for enhancing the accuracy of low-cost receivers by single-frequency relative kinematic positioning. *Measurement Science and technology* 24 (11): 115010.
- Sun R, Hsu L-T, Xue D, et al. (2018) GPS Signal Reception Classification Using Adaptive Neuro-Fuzzy Inference System. *Journal of Navigation*: 1-17.
- Suzuki T and Kubo N. (2013) Correcting GNSS Multipath Errors Using a 3D Surface Model and Particle Filter. *Proceedings of the 26th International Technical Meeting of the Satellite Division of The Institute of Navigation (ION GNSS+ 2013)*: 1583-1595.
- Suzuki T and Kubo N. (2014) N-LOS GNSS signal detection using fish-eye camera for vehicle navigation in urban environments. *27th International Technical Meeting of the Satellite Division of the Institute of Navigation, ION GNSS 2014* 3: 1897-1906.
- Wang L, Groves PD and Ziebart MK. (2012) Multi-Constellation GNSS Performance Evaluation for Urban Canyons Using Large Virtual Reality City Models. *Journal of Navigation* 65 (3): 459-476.
- Wang L, Groves PD and Ziebart MK. (2013) GNSS Shadow Matching: Improving Urban Positioning Accuracy Using a 3D City Model with Optimized Visibility Scoring Scheme. *Navigation*. 195-207.
- Wen W, Zhang G and Hsu L-T. (2018a) Correcting GNSS NLOS by 3D LiDAR and Building Height. *Proceedings of the 31st International Technical Meeting of the Satellite Division of The Institute of Navigation (ION GNSS+ 2018)*: 3156-3168.
- Wen W, Zhang G and Hsu L. (2018b) Exclusion of GNSS NLOS receptions caused by dynamic objects in heavy traffic urban scenarios using real-time 3D point cloud: An approach without 3D maps. *2018 IEEE/ION Position, Location and Navigation Symposium (PLANS)*. 158-165.
- Xu B, Jia Q, Luo Y, et al. Intelligent GPS L1 LOS/Multipath/NLOS Classifiers based on Correlator, RINEX and NMEA-level Measurements. *Remote Sensing*: (Accepted).
- Ziedan NI. (2017) Urban Positioning Accuracy Enhancement Utilizing 3D Buildings Model and Accelerated Ray Tracing Algorithm. *Proceedings of the 30th International Technical Meeting of The Satellite Division of the Institute of Navigation (ION GNSS+ 2017)*: 3253 - 3268.

